Classification of Underwater Objects based on Zernike and Pseudo Zernike Moments and Fourier Descriptors

Vorlage für Studentenarbeiten
Bachelor-Thesis von Javier Arpon Diaz-Aldagalan
30. September 2010

TECHNISCHE
UNIVERSITÄT
DARMSTADT

Classification of Underwater Objects based on Zernike and Pseudo Zernike Moments and Fourier Descriptors
Vorlage für Studentenarbeiten

Vorgelegte Bachelor-Thesis von Javier Arpon Diaz-Aldagalan

1. Gutachten: Raquel Fandos
2. Gutachten: Prof. Dr.-Ing. A. Zoubir

Tag der Einreichung:

Declaration / Erklärung

To the best of my knowledge and belief this work was prepared without aid from any other sources except where indicated. Any reference to material previously published by any other person has been duly acknowledged. This work contains no material which has been submitted or accepted for the award of any other degree in any institution.

Hiermit versichere ich die vorliegende Arbeit ohne Hilfe Dritter nur mit den angegebenen Quellen und Hilfsmitteln angefertigt zu haben. Alle Stellen, die aus Quellen entnommen wurden, sind als solche kenntlich gemacht. Diese Arbeit hat in gleicher oder ähnlicher Form noch keiner Prüfungsbehörde vorgelegen.

Darmstadt, den 30. September 2010

(Javier Arpon Diaz-Aldagalan)

Abstract

In this work the process of classification of underwater objects in sonar images is treated. The necessary steps, which are based on image processing and computer vision, are first the segmentation, then feature extraction and finally classification.

Three different kinds of descriptors are tested in this work: the Zernike Polynomials (ZP), the pseudo Zernike Polynomials (PZP) and the Fourier Descriptors (FD).

Several sets of these coefficients are tested with a Mahalanobis classifier.

A set of coefficients are proposed that give us succesful results for each feature descriptor and there are compared to choose the most reliable.

Abbreviations, Acronyms and Symbols

A_{nm}	Complex Zernike moments
f	Feature vector
F_{uv}	2-D Discrete Fourier Transform
I	Image
$\mathcal{N}_x$	Gaussian distribution
$\mathscr{P}_c$	PDF of feature vectors
R_{nm}	Radial Polynomials of Zernike polynomials
R'_{nm}	Radial Polynomials of Pseudo Zernike polynomials
V_{nm}	Zernike Polynomials
μ	Mean value
$\sum$	Covariance matrix

Contents

List of Figures

List of Tables

1 Introduction

A naval mine is a self-contained explosive device placed in water to destroy ships or submarines. Unlike depth charges, mines are placed and left to wait until they are triggered by the approach of an enemy ship. Mines can be inexpensive: some variants can cost as little as a thousand euros, although more sophisticated mines can cost millions of euros. The cost of producing and laying a mine is between 0.5 % and 10 % of removing it, and it can take up to 200 times more to clear a minefield than to lay it. For example parts of some World War II naval minefields still exist, because they are too extensive and expensive to clear; some of these mines might remain dangerous for hundreds of years. For this reason, the detection and removal of mines is a global problem and it is important to do research in this field.

The use of sonar images for underwater mine detection is relatively recent because until a few years ago the information that sonar contributed was limited, with the advance of technology this devices have managed to obtain considerably sharper images.

Figs. 1.1 and 1.2 show two typical underwater mines. The first one corresponds to a spherical mine and the second to a cylindrical mine. The results of segmenting this images using a Markov Random Fields algorithm [16] are shown in Figs. 1.3 and 1.4, respectively. Three different regions are observed: the highlight of the object (in green), the shadow of the object (in red) and the background (in blue).

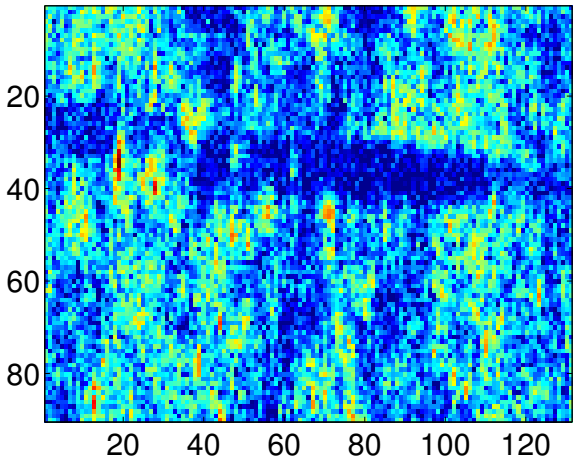

Figure 1.1: Sonar image of spherical mine

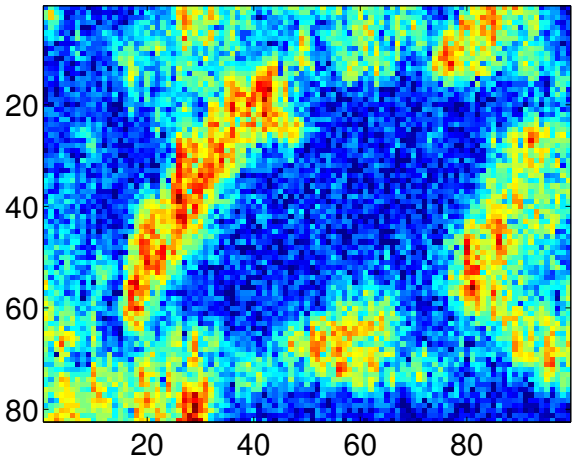

Figure 1.2: Sonar image of cylindrical mine

Typically, a spherical mine consists of a more or less round highlight and an ellongated shadow, while cylindrical mines consist of ellongated objects and rhomboid like shadows.

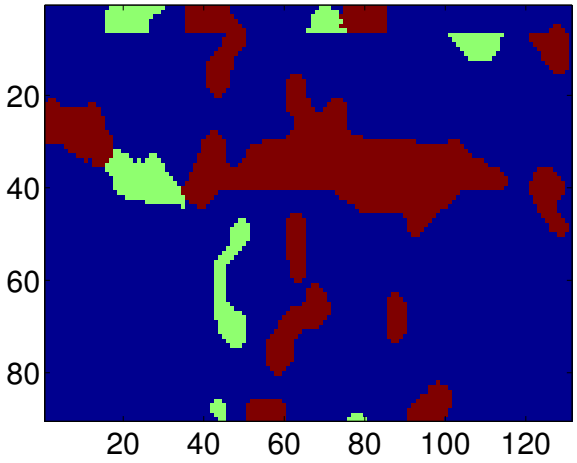

Figure 1.3: Segmented image of the spherical mine in Fig. 1.1

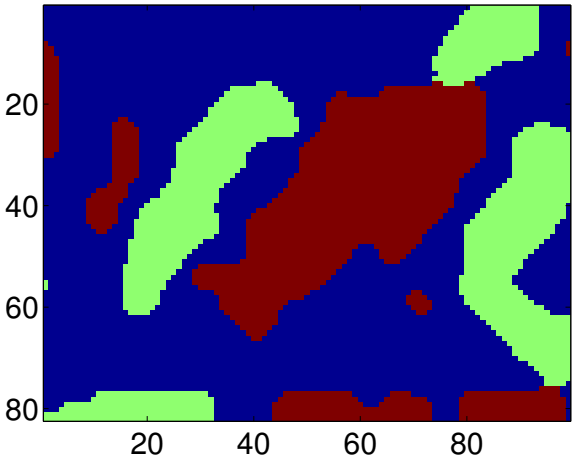

Figure 1.4: Segmented image of the cylindrical mine in Fig. 1.2

Due to the variability of the object highlights, the classification of underwater objects has traditionally been made considering features of the shadow region [1, 6, 29]. This is also the approach adopted in this work.

Three families of geometrical descriptors have been considered: Zernike Polynomials (ZP), pseudo Zernike Polynomials (PZP) and Fourier Descriptors (FD). Different sets of these descriptors have been tested with a database of segmented images. The database consists of 131 cylindrical mines, 320 spherical mines and 3868 'no mine' objects, that is, regions of the seabed that are segmented but that do not correspond to a mine object. In Figs. 1.5a and 1.5b two examples of these 'no mine' objects are shown. Applying the segmentation algorithm to them results in the segmented images in Figs. 1.6a and 1.6b respectively.

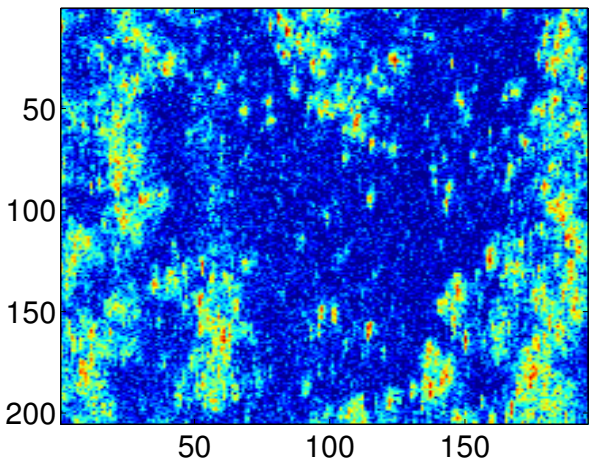

(a) Example 1 'no mine'

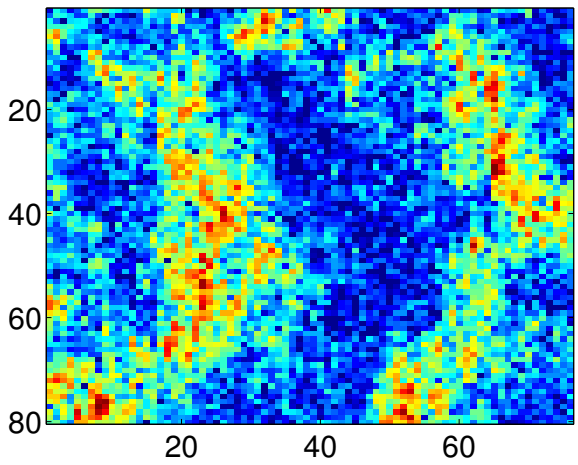

(b) Example 2 'no mine'

Figure 1.5: Examples of 'no mine' objects

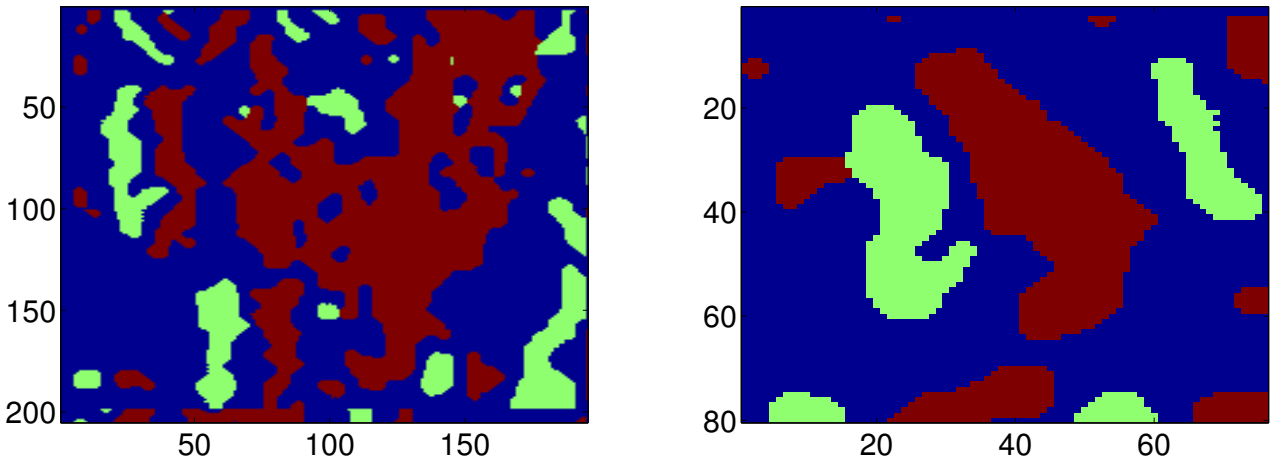

(a) Segmented image 'no mine' 1 (b) Segmented image 'no mine' 2

Figure 1.6: Segmented images of upper 'no mine' objects

Hence, the objective of this work is to choose the set of descriptors that produces the best classification results for the available database, that is, that maximizes the correct classification of both cylindrical and spherical mines while keeping a low probability of false alarm.

In Fig. 1.7 a scheme of the system is depicted.

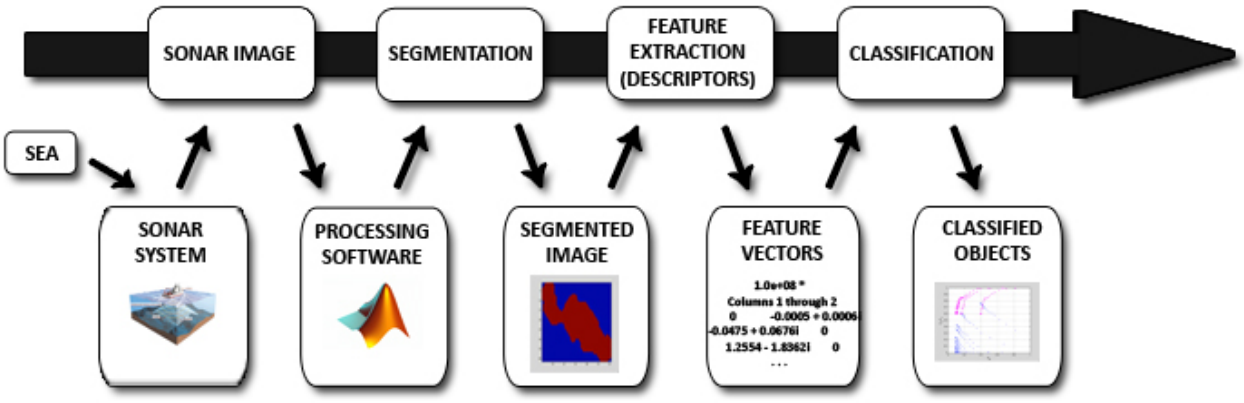

Figure 1.7: Sketch of the process of classification

The first step is obtaining the sonar image by a beam forming algorithm. Subsequently, this image is treated with the computer software Matlab®. The image is segmented [2, 8, 30] and the object shadow is obtained. This thesis starts here, because we begin with the segmented image as input. Once separated the shades, they are different descriptors [4, 35] used for get information about these shadows to obtain features vectors of the different types of objects. These vectors

are used by the classifier [12, 20, 37] implemented to separate the objects into the three different classes: spherical mine, cylindrical mine and 'no mine'.

The structure of this thesis follows this structure:

In chapter 2: here are introduced all the descriptors used as well as the implementation of them.

In chapter 3: in this section the classifier is explained.

In chapter 4: this episode contains the results and graphics of the proofs executed, also are included comments and tables.

Finally in chapter 5: in the last point is presented a little conclusion about the work and the results

2 Descriptors

As has been mentioned earlier, the purpose of the descriptors is to characterize the shadows of the three types of objects. There are different kinds of descriptors, such as contour-based or region-based. In this work we have chosen to use the following region-based descriptors: Zernike and pseudo Zernike moments and Fourier Descriptors. These have been used according to [5, 36, 38]. They are selected for their better performance.

2.1 Definition and implementation of Zernike Polynomials

The applications of orthogonal moments based on Zernike Polynomials for image processing were pioneered by Teague [33] in 1980. He proposed the use of these orthogonal moments to recover the image based on the theory of orthogonal polynomials, and has introduced Zernike moments which allow independent moment invariants to be constructed to an arbitrarily high order.

These moments have simple rotational transformation properties so the magnitudes of the Zernike moments (ZM) of a rotated image remains identical to the original function. Thus the magnitude of the Zernike moment, $|A_{nm}|$, can be employed as a rotation invariant feature of the image.

A set of orthogonal functions with simple rotation properties which forms a complete orthogonal set over the interior of the unit circle was introduced by Zernike [11]. The form of these polynomials is

$$V_{nm}(x,y) = V_{nm}(\rho \sin\theta, \rho \cos\theta) = R_{nm}(\rho) \exp(jm\theta), \tag{2.1}$$

where n is either a positive integer or zero, and m takes positive and negative integer subject to constraints $n - |m| =$ even, $m \leq n$, ρ is the length of the vector from the origin to the pixel at position (x,y), and θ is the angle between vector ρ and the x axis in the counterclockwise direction.

The radial polynomial $R_{nm}(\rho)$ is defined as

$$R_{nm}(\rho) = \sum_{s=0}^{(n-|m|)/2} (-1)^s \frac{(n-s)!}{s!(\frac{n+|m|}{2}-s)!(\frac{n-|m|}{2}-s)!} \rho^{(n-2s)} \tag{2.2}$$

$$= \sum_{s=0}^{(n-|m|)/2} Z_{nms}\, \rho^{(n-2s)} \tag{2.3}$$

with $R_{n,-m}(\rho) = R_{n,m}(\rho)$.

Zernike polynomials are a complete set of complex-valued function orthogonal over the unit disk. The complex Zernike moments of order n with repetition m for an image $I(x,y)$ are defined as

$$A_{nm} = \frac{n+1}{\pi} \sum_x \sum_y I(x,y) V^*_{nm}(x,y), \tag{2.4}$$

where * means complex conjugate. Due to the conditions $n - |m| =$ even, and $m \leq n$ for the Zernike polynomials in Eq. (2.1).

Since $A^*_{nm} = A_{n,-m}$ then $|A_{nm}| = |A_{n,-m}|$, therefore, one only needs $|A_{nm}|$ with $m \geq 0$.

To implement the Zernike coefficients, we first obtain a database with Z_{nms}, $0 \leq n \leq N_{max}$, $m \leq n$, since they do not depend on the image. After, ρ and θ are found for each pixel of the image under consideration. With these data it is possible to apply the general formula of Zernike polynomials over the image.

In the implementation, for values of n greater than or equal to 45, the computer software Matlab® presents accuracy problems. This in however not critical for our application since, as presented in chapter 4, 10 coefficients are enough for our purpose.

This Zernike polynomials contain linearly independent $\frac{1}{2}(N_{max}+1)(N_{max}+2)$ polynomials being N_{max} the maximum index.

2.2 Definition and implementation of Pseudo Zernikes Polynomials

Pseudo Zernike polynomials is similar than Zernike polynomials. The differences between them are two. These was derived by Bhatia and Wolf [3]. The first is that it must to eliminate the condition $n - |m| =$ even regarding the ZP defined in Sec. 2.1.

The second is that the radial polynomial equation changes slightly from the Eq. (2.2),

$$R'_{nm}(\rho) = \sum_{s=0}^{n-|m|} (-1)^s \frac{(2n+1-s)!}{s!(n-|m|-s)!(n+|m|+1-s)!} \rho^{(n-s)}, \tag{2.5}$$

where $n = 0,1,2, ...,\infty$ and m takes on positive and negative integers subject to $|m| \leq n$. This set of pseudo-Zernike polynomials contains $(N_{max}+1)^2$ linearly independent polynomials if the given maximum order is N_{max}.

Since the set of pseudo Zernike orthogonal polynomials is analogous to that of Zernike polynomials, most of the previous discussion for the ZM can be adapted to the case of pseudo Zernike Moments (PZM).

Summing up, the way to implement the PZM is analogous to ZM, therefore we rely on the files already generated, here the difference is mainly in the conditions, because we eliminate the condition $n-|m| =$ even and change our way of finding the R_{nm} and we use the equation Eq. (2.5).

2.3 Definition and implementation of Fourier Descriptors

In many applications of pattern recognition and digital image processing Fourier Descriptors (FD) are used [24]. This feature is based on the Fourier transform in two dimensions. FD of the shape are formed by the Fourier coefficients, so the shape of the object is represented in a frequency domain with these descriptors.

The Fourier coefficients of low order contain information about the general features of the shape. Whereas, the higher frequency descriptors contain information about more accurate details of the shape.

The way to obtain these coefficients is using the two-dimensional DFT:

$$F_{uv} = \frac{1}{NM} \sum_{x=0}^{N-1} \sum_{y=0}^{M-1} I(x,y) e^{-2\pi i \left(\frac{xu}{N} + \frac{yv}{M}\right)}, \tag{2.6}$$

where N and M are the number of samples in the two dimensions and the Discrete Fourier transform in 2D of the shape is F_{uv}.

The phase of the Fourier coefficients provides information about orientation and the symmetry of the regions.

3 Classification

The third chapter contains how the classifier works. The objective is to study the performance of different sets of features to classify underwater objects as man made or natural objects. Thus, the objective for is to separate the objects into three groups corresponding to 'spherical mines' (S), 'cylindrical mines' (C) and 'no mines' (N). We want to specially focus in false alarms, which are the most important data. We try that when a 'no mine' is considered as a mine, the correct mine detection rate would be as high as possible. The purpose is to choose the best descriptors and coefficients for achieve the most successful results.

3.1 Definition of the classifier

For the features vectors classification Mahalanobis Classifier is used. This is chosen because it can often solve problems caused by poorly scaled and/or highly correlated features.

It is assumed for simplicity, that the vectors have a Gaussian distribution. If a random variable X has a Gaussian distribution, it is written as $X \sim \mathcal{N}(\mu, \sum)$ or to make it explicitly known that X is k-dimensional,

$$\mathcal{N}_k(\mu, \sum), \tag{3.1}$$

with k-dimensional mean vector:

$$\mu = \left[E[X_1], E[X_2], ..., E[X_k]\right], \tag{3.2}$$

and k x k covariance matrix

$$\sum = \left[Cov[X_i, X_j]\right]_{i=1,2,...,k; j=1,2,...,k} \tag{3.3}$$

Returning to our project, it is assumed that feature vectors follows the next equations:

$$f = (f_1, \cdots, f_L) \sim \mathcal{N}(\mu_c, \sum_c), \tag{3.4}$$

where f is a feature vector of L elements. Hence, the probability density function (pdf) of the feature vector f, P_C, depends on the class, where $c = N, S, C$.

And the next one represents the probability distribution function of these vectors:

$$\mathscr{P}_c = \frac{1}{(2\pi)^{\frac{k}{2}} |\sum|^{\frac{1}{2}}} \exp^{-\frac{1}{2}(f - \mu)' \sum^{-1} (f - \mu)}, \tag{3.5}$$

where $\mathcal{N}(\mu_c, \sum_c)$ is a normal distribution with mean μ and covariance $\sum$, and $|\cdot|$ denotes the determinant.

The following figures (3.1a 3.1b 3.1c) are three examples of Gaussian curves of different classes of objects in the three descriptors used.

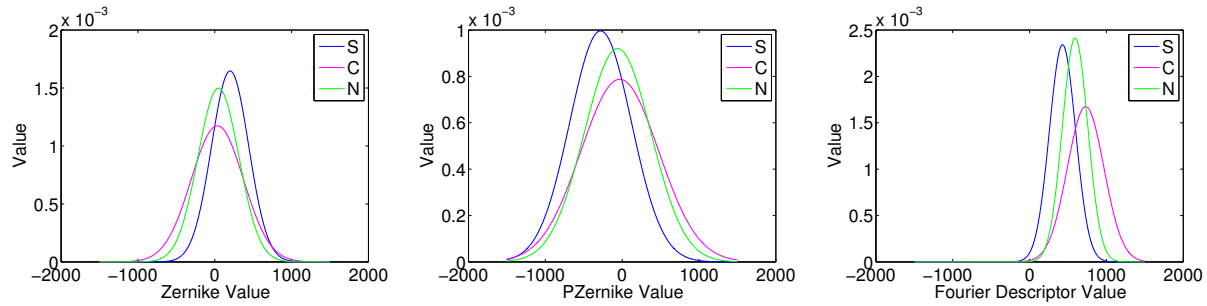

(a) ZM (coeffs. n=4 m=4) (b) PZM (coeffs. n=5 m=4) (c) FD (coeff. 0,0)

Figure 3.1: Gaussian Curves of different classes

To sort the probabilities obtained what is done is to compare the results obtained by the following equations (Eq. (3.6)) with variable thresholds. In the Fig. 3.2 it can be seen three colors representing realizations of f for the three different classes, assuming that $L = 2$. The thresholds are the black lines. The classification depends on the movements of these thresholds. The object is considered to be part of one of the three groups. This finally allows to represent the correct probability of detect the type of the mine versus the false alarm rate, as shown in Fig. 3.3.

$$\begin{aligned} \frac{\mathscr{P}_C(f_i)}{\mathscr{P}_N(f_i)} &\gtrless T_{CN} \\ \frac{\mathscr{P}_C(f_i)}{\mathscr{P}_S(f_i)} &\gtrless T_{CS} \end{aligned} \tag{3.6}$$

These are an example of classify the cylindrical objects, but the process is the same for the others types of mines.

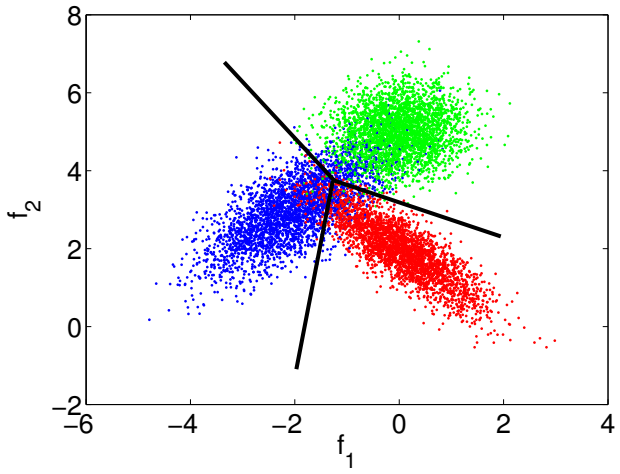

Figure 3.2: Probabilities and thresholds

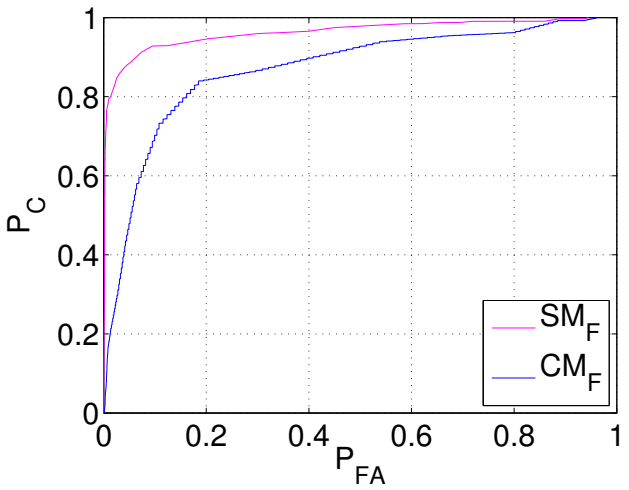

Figure 3.3: Example of classification curves

The leave-one-out technique is used, this means that when we want to compare an image, it is left out when calculating the values to find the distribution, for example, if we want to work with the first image of spherical-mines' database, we take all the images except that (the first one) to find μ and $\sum$.

4 Results

In this chapter we present the classification results obtained for the different sets of descriptors. The first part shows the comparison between Zernike (ZM) and Pseudo Zernike moments (PZM). Subsequently, these two and the Fourier descriptors (FD) are presented separately. Finally the best results of each descriptor are presented together.

All figures represent on the X axis the probability of false alarm (P_{FA}), that is, the probability of classify a 'no mine' object as a mine. On the Y axis it is represented the probability of correct classification of the mine objects (P_C), both spherical (magenta line) and cylindrical mines (blue line).

4.1 Zernike moments vs. Pseudo Zernike moments

In this section it has been used index $n = 0..10$ and $m = 0..10$ and they have been sufficient to achieve good results as shown later.

This comparison of ZM versus PZM represent the minimum values obtained by the descriptors which means that effectiveness in the classification is actually higher.

In these figures the representation is a little different: on the Y axis the correct probabilities of classification (P_C), on the X axis false alarm probability (P_{FA}). In magenta color is represented the ZM curve and in blue color the PZM curve.

Comparisons have been made by orders, this means that it has been chosen the coefficients that their sum of index n and m are the same. As to display the order for 0, 2, 4, 6, 8, 10 and 12, but the last one is not quite correct because lack of the polynomials corresponding to 11 and 12 because we start from 0 to 10 polynomials for n and equal to m.

Fig. 4.1 of this section that corresponds to the order 0, one can distinguish only one line and this is because ZM and PZM corresponding to (0,0) is the same for both, and get very poorly result, only reaching in the middle-graph 50 % of reliability.

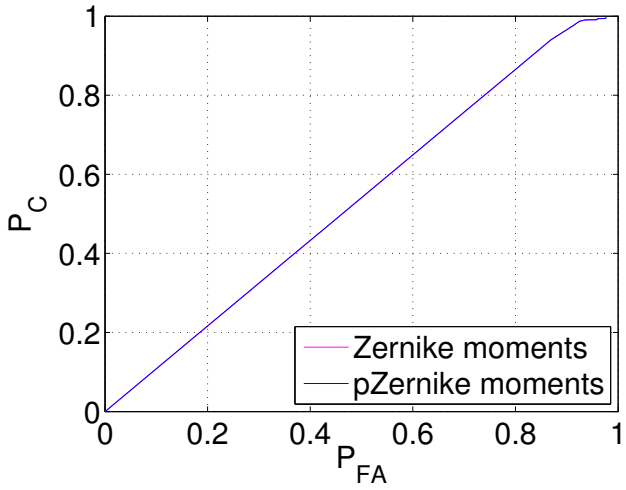

Figure 4.1: ZM vs. PZM order 0

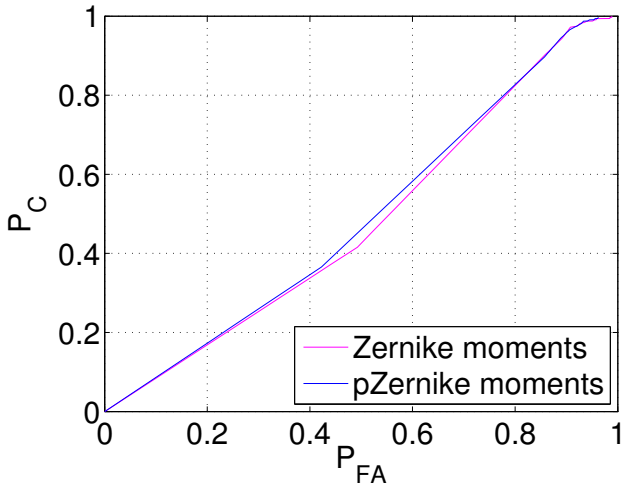

Figure 4.2: ZM vs. PZM order 2

In the figure of order 2 (Fig. 4.2), that corresponds to the polynomials (1,1) and (2,0), the difference between ZM and PZM can be seen already, where the response of the latter is slightly worst, we have now only 40 % of minimum detection when we have 50 % of probability of false alarm.

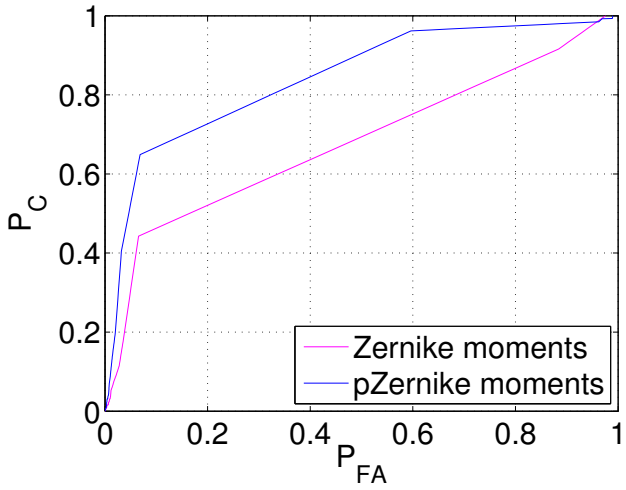

Figure 4.3: ZM vs. PZM order 4

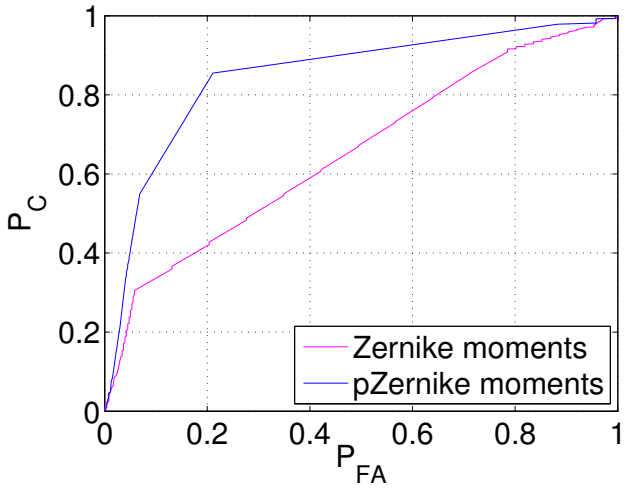

Figure 4.4: ZM vs. PZM order 6

In Fig. 4.3 is shown the performance of the moments of order 4, corresponding to the coefficients (2,2), (3,1) and (4,0), they achieve better results, is seen as rising faster slopes, and now is getting up to 80 % of correct detection when we have 30 % of probability of type mine classification in the case of PZM. The ZM continue under the PZM, nearly 20 % of difference.

Fig. 4.4 corresponds to the coefficients (3,3), (4,2), (5,1) and (6,0) (order 6). It can be seen as PZM improves reaching almost 90 % of probability of correct classification when we only have a 20 % rate of false alarm. However, the performance of ZM does not improve.

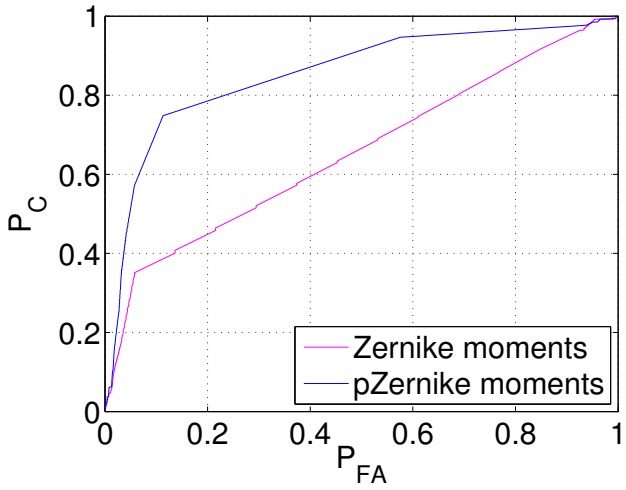

Figure 4.5: ZM vs. PZM order 8

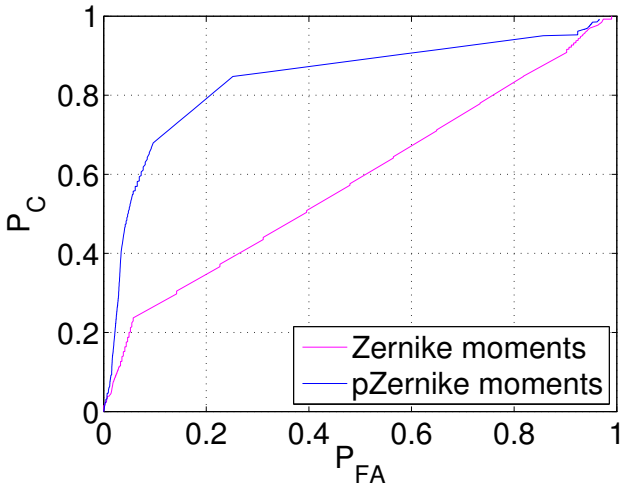

Figure 4.6: ZM vs. PZM order 10

In the Fig. 4.5 we have the coefficients of order 8 ((4,4), (5,3), (6,2), (7,1) and (8,0)), values fall slightly.

Regarding the data of order 10 which can be seen in Fig. 4.6 (corresponding to the coefficients (5,5), (6,4), (7,3), (8,2), (9,1), (10,0)) it can be seen that ZM are worse and PZM continue more or less the same.

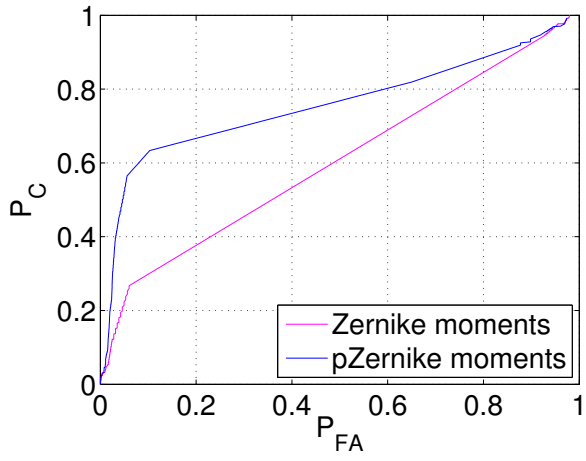

Figure 4.7: ZM vs. PZM order 12

In the Fig. 4.7 the set of order 12 is represented (coefficients (6,6), (7,5), (8,4), (9,3) and (10,2), it should be noted that as discussed on the first paragraph, the coefficients (11,1) and (12,0) are missed because they have only been treated to the (10,10)). Both ZM and PZM behave worse, specially the last ones which are despised around 10 %; the results we provide are lower, so it does not consider it relevant to look at higher orders.

Summing up the graphs and reviews so far, if we seek the order that best works for the two descriptors at a time, the order 4 is selected, while if we choose the best descriptor, this would be the PZM of order 6 or 8. Recalling that represent the worst values of each order, this gives us to think that generally the results will be so better, as discussed in the following subsections of this chapter.

Figs. 4.8 and 4.9 correspond to the comparison of some coefficients that have been selected not by orders. These first coefficients are chosen because have the maximum information as we can obtain.

It will present square areas of coefficients for ZM and for PZM as they are shown in the images, according to the conditions set out in chapter 2.1 and 2.2 as $n > m$ for both of them and $n - m = even$ only for ZM.

In the images a different colour represents the new coefficients chosen for the chart.

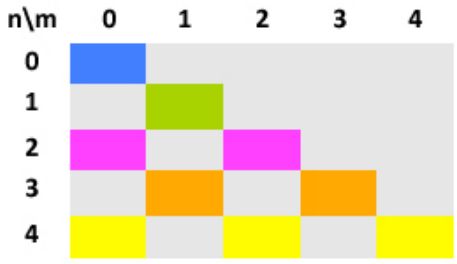

Figure 4.8: ZC chosen

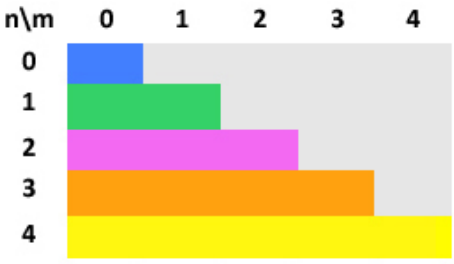

Figure 4.9: PZC chosen

The first selection of coefficients according to the diagram shown would be the (0,0) (order 0) but it is already commented and corresponds to the Fig. 4.1. The Fig. 4.10 represents the coefficients group: (0,0) and (1,0) for ZM and (0,0), (1,0) and (1,1) for PZM. It is seen that the response is bad for both, specially for PZM.

In Fig. (4.11) the coefficients (2,0) and (2,2) for ZM and (2,0), (2,1) and (2,2) for PZM have been added. A probability of 90 % of correct classification with a 20 % probability of false alarm is achieved in the case of PZM. We can see how the responses of the descriptors are better than any orders treated before.

If we look at the Fig. 4.12 it can be seen that what it is got is a faster slope. The effectiveness is very similar but the slope rises faster and achieves on 80 % success rate with only 10 % confidence that it is mine. In this case the added coefficients as shown in the diagram are for ZM (3,1) and (3,3), and for PZM (3,1), (3,2) and (3,3).

The last graph of this group, corresponding to the added coefficients (4,0), (4,2) and (4,4) for ZM and (4,0), (4,1), (4,2), (4,3) and (4,4) for ZPM. It is got a slope even more abrupt but the data obtained from the graph are very similar to the graph above (4.12) in which we use three and five coefficients respectively less so that is more efficient.

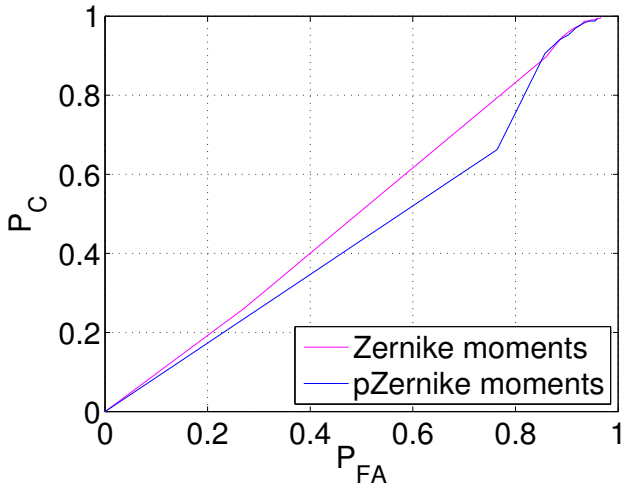

Figure 4.10: ZM vs. PZM n=0..1 m=0..1

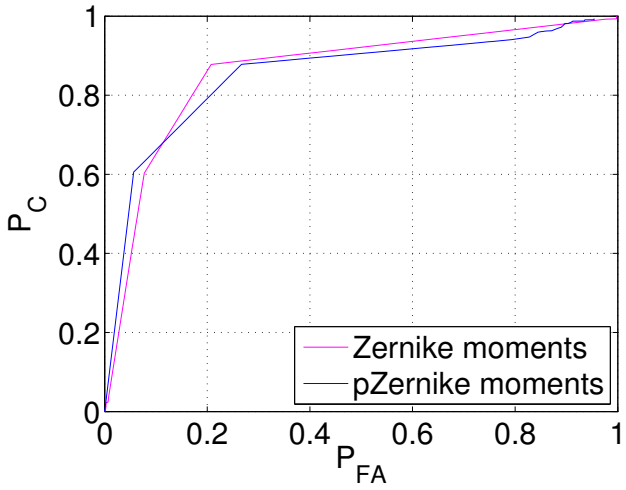

Figure 4.11: ZM vs. PZM n=0..2 m=0..2

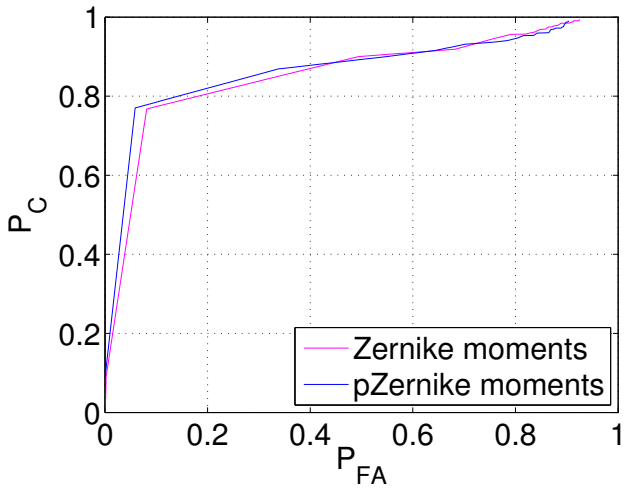

Figure 4.12: ZM vs. PZM n=0..3 m=0..3

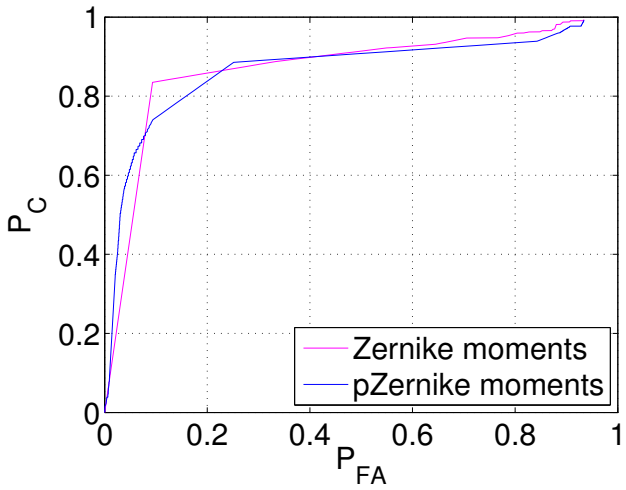

Figure 4.13: ZM vs. PZM n=0..4 m=0..4

With this group of graphs which is intended to highlight is that the choice of coefficients according to the results of ZM and PZM are very similar and respond well. It must be remarked how has been done so far, these are the low rates of classification. In the following sections, the correct classification is separated in two different curves that represent spherical mines and cylindrical mines respectively.

This section presents the individual results of ZM. Where before have drawn the results of ZM and PZM curves, now they are displayed separately spherical (SM) and cylindrical mines (CM) in relation with be a false alarm.

In Fig. 4.14 examples are shown of each of the three types of underwater objects: SM, CM and NM. Below, in Fig. 4.15 are rendered the ZM of their upper images.

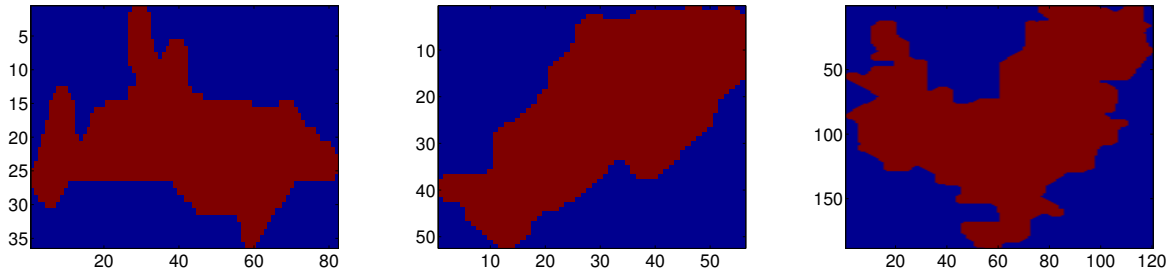

(a) Spherical mine (b) Cylindrical mine (c) No mine

Figure 4.14: Examples of different types of objects

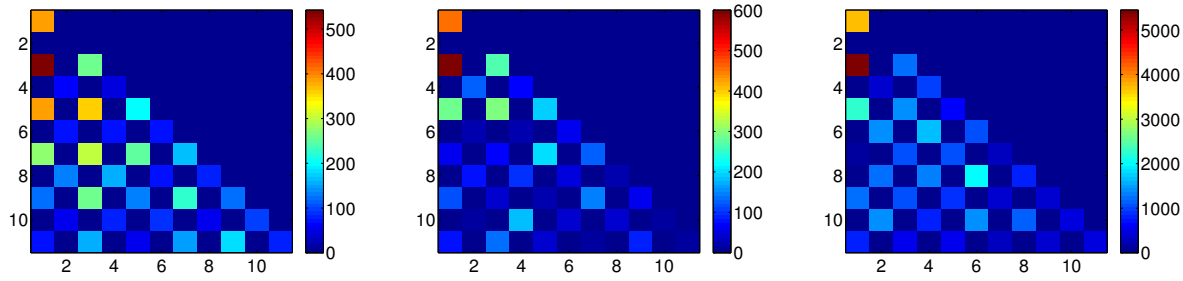

(a) ZM for upper (b) ZM for upper (c) ZM for upper

Figure 4.15: ZM obtained for 4.14

In the Fig. 4.16 which are represented the ZM of order 2, it is seen that they respond with the best behavior for cylindrical mines getting a 50 % of probability of detection while spherical mines have a 10 % when it has a 10 % of probability of false alarm.

Fig. 4.17 gets much better results, the slopes are higher, and now including spherical mines are located above the cylindrical ones, taking for example with a 20 % of probability of false alarm, 75 % and 52 % of probability respectively.

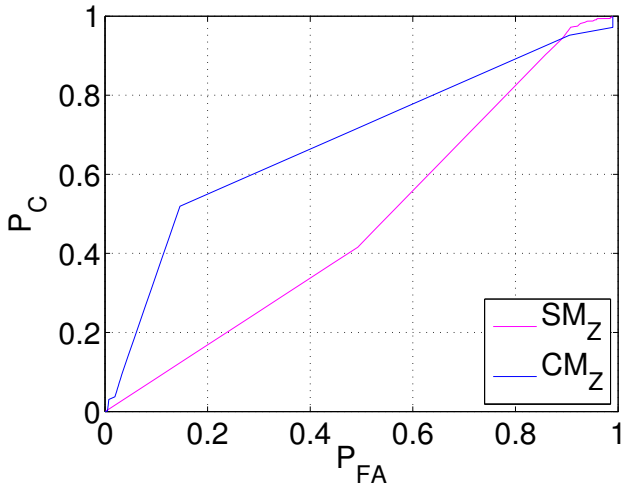

Figure 4.16: ZM order 2

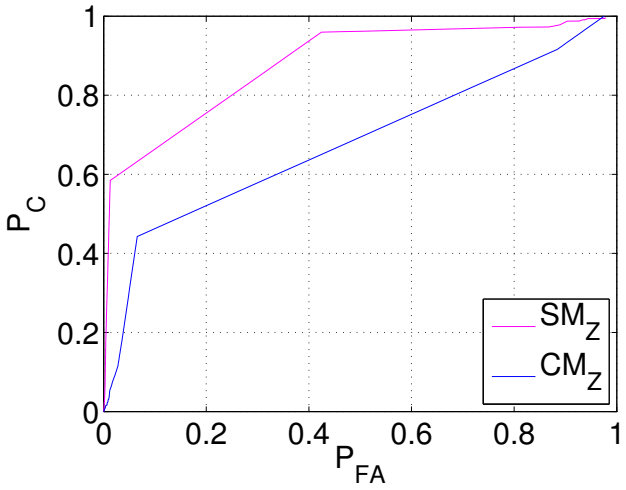

Figure 4.17: ZM order 4

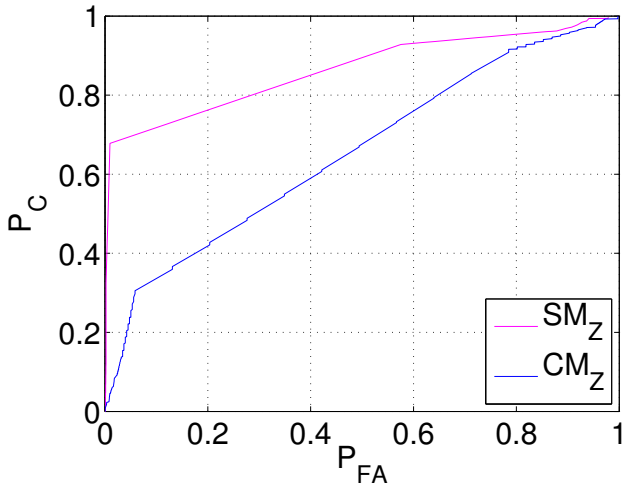

Figure 4.18: ZM order 6

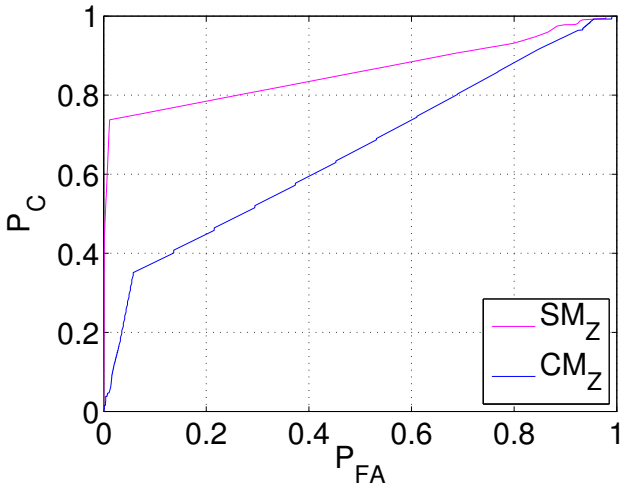

Figure 4.19: ZM order 8

As it can be seen in the Fig. 4.18 the spherical mines improve their results and now they get have 70 % of reliability with only 3 % of possibility of false alarm. Although, the cylindrical mines rate decrease their values on 10 % respecting the previous figure.

In Fig. 4.19 the values improve at the begining a little but later the results are more or less than the results of order 6.

It can be seen in Fig. 4.20 as the two lines corresponding to the coefficients of order 10 worse their response, their answers are still quick with a high elevation in the first points, but lose inclination in the rest of the graph.

Almost no noticeable improvement in graphics 4.21. Results are practically the same than the Fig. 4.20 of order 10. It has to noticed that the coefficients (11,1) and (12,0) are missed on this figure but they are so high so would not improve the outcome, so they are scorned.

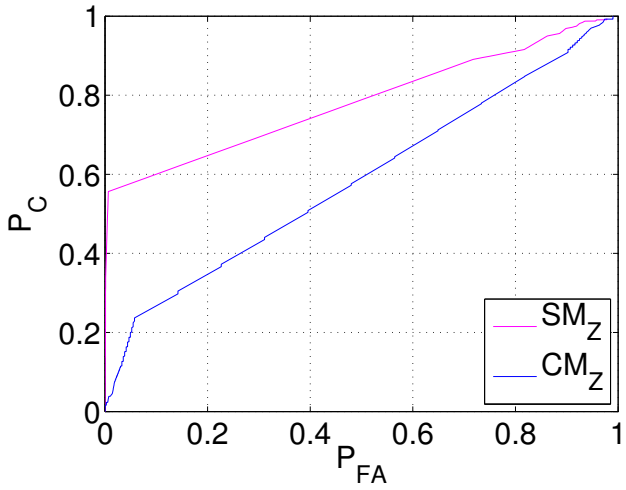

Figure 4.20: ZM order 10

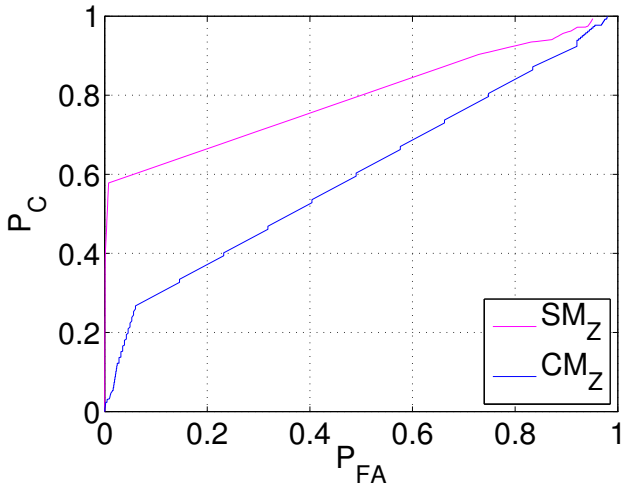

Figure 4.21: ZM order 12

After seeing the figures of the coefficients chosen in order, now are being display the graphs of the coefficients chosen according to the figure 4.8 that are covering an ever bigger index n and m in each graph.

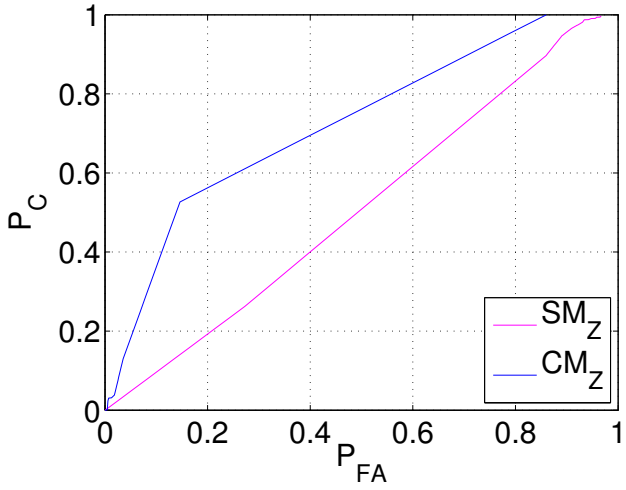

Figure 4.22: ZM n=0,1 m=0,1

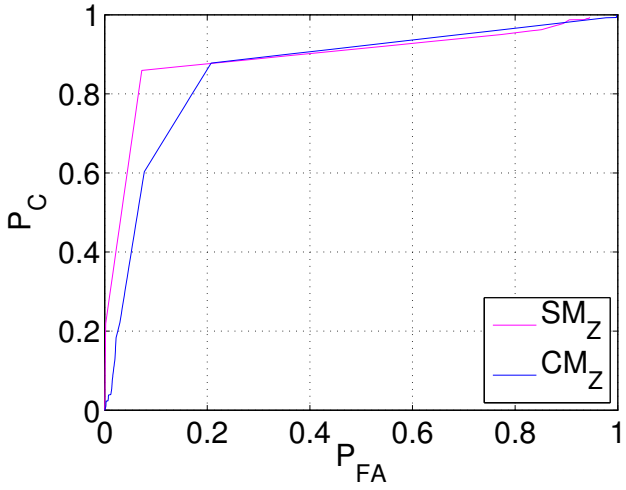

Figure 4.23: ZM n=0..2 m=0..2

The Fig. 4.22 corresponds to the coefficients (0,0) and (1,1) and is very similar to the graph of order 2 as the coefficients of it are (1,1) and (2,0), so that changes only in one of them. The results are not as good as those provided by other groups of coefficients.

In Fig. 4.23 it is noticeable the improvement, getting when we have 20 % of probability of false alarm, about 90 % of probability of detection for each type of mine, indicating very good results with this coefficient group: (0,0), (1,1), (2,0) and (2,2).

The Fig. 4.24 yields a slightly faster response than the previous figure, but they are loosen good results before the middle of the chart while after this point the results are a little better.

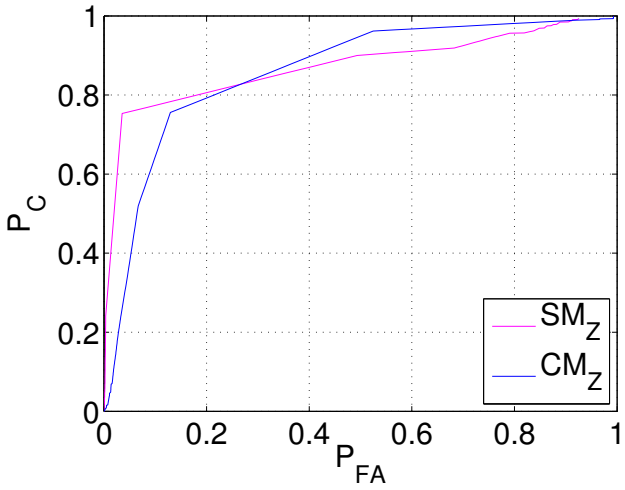

Figure 4.24: ZM n=0..3 m=0..3

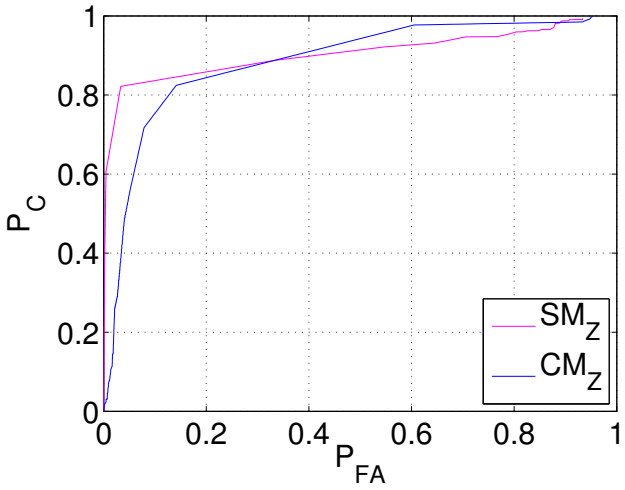

Figure 4.25: ZM n=0..4 m=0..4

And in the last figure of the group, the Fig. 4.25 obtains a little faster results, but it is noticed that the data begins to not vary much because they are already considerably effective.

To sum up this section on ZM behavior, it is noteworthy that overall the results offered by the coefficients treated (which are 11x11), these are sufficient and effective for our purpose. The descriptor obtains a high probability of success of detect the correct type of mine having a slight probability of false alarm.

And considering the effect on the minimum number of coefficients selected, Fig. 4.23 corresponding to (0,0), (1,1), (2,0) and (2,2) is the most effective.

It has been proved that the coefficients selected according to Fig. 4.8 respond better than the coefficients chosen by orders.

This section mentions the results of Pseudo Zernikes coefficients chosen by order and then the ones according to Fig. 4.9 as has been done so far.

Fig. 4.26 shows examples of a spherical mine, a cylindrical mine and a 'no mine'. Below, in Fig. 4.27 are drawn the PZM of their upper images.

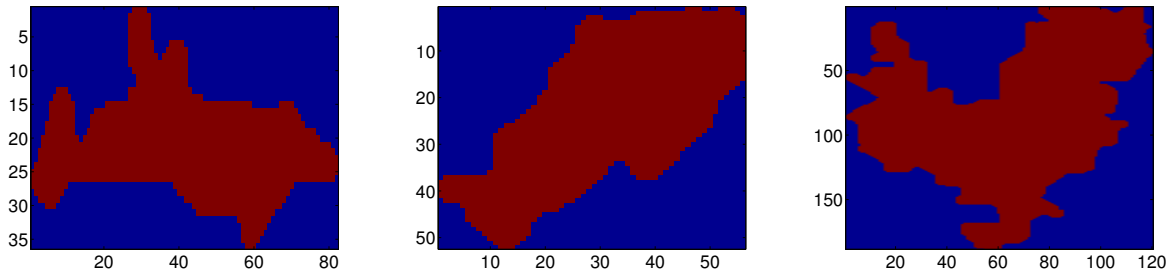

(a) Spherical mine (b) Cylindrical mine (c) No mine

Figure 4.26: Examples of different types of objects

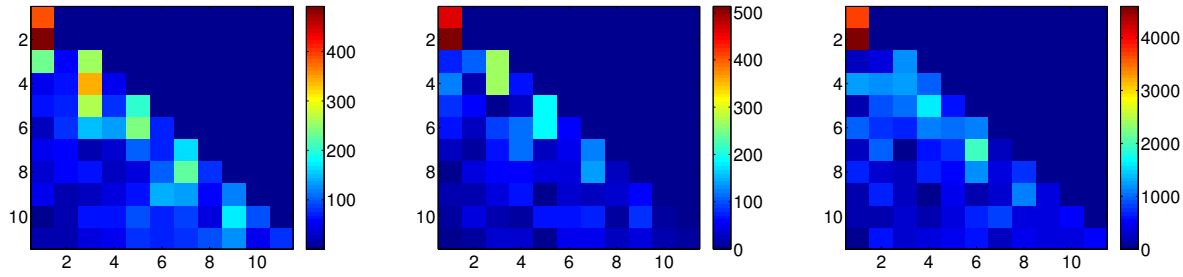

(a) PZM for upper (b) PZM for upper (c) PZM for upper

Figure 4.27: PZM obtained for 4.26

First we discuss the figures of the coefficients chosen by order. We start with order 2 corresponding of coefficients (2,0) and (1,1) (Fig. 4.28). It is seen that the descriptor responds with very low results on spherical mine detection, while in cylindrical mine detection get 60 % probabiity with only 20 % probability of false alarm. The difference between the descriptors are near of 35% what is too much for our purpose. As mentioned before, coincides with the results of the ZM of order 2 (Fig. 4.16).

In the figure 4.29 corresponding to the coefficients of order 4, one can see a big change from the previous figure, now spherical mines and cylindrical mines classifiers respond almost the same, obtaining 70 % of reliability with 20 % of false alarm.

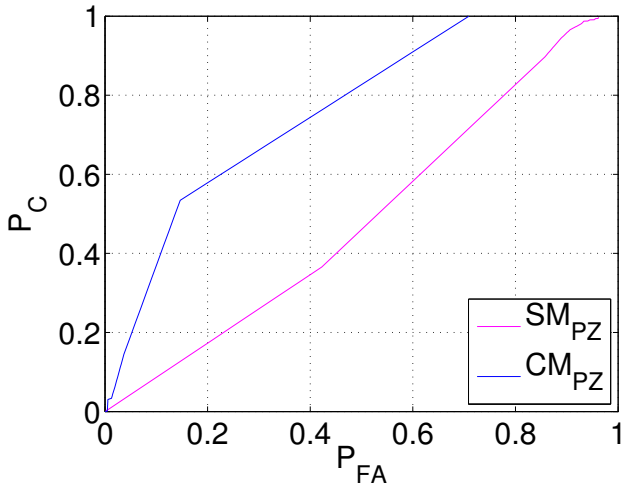

Figure 4.28: PZM order 2

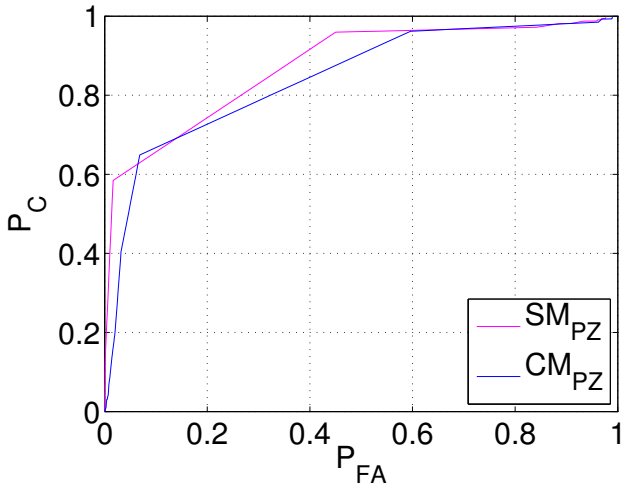

Figure 4.29: PZM order 4

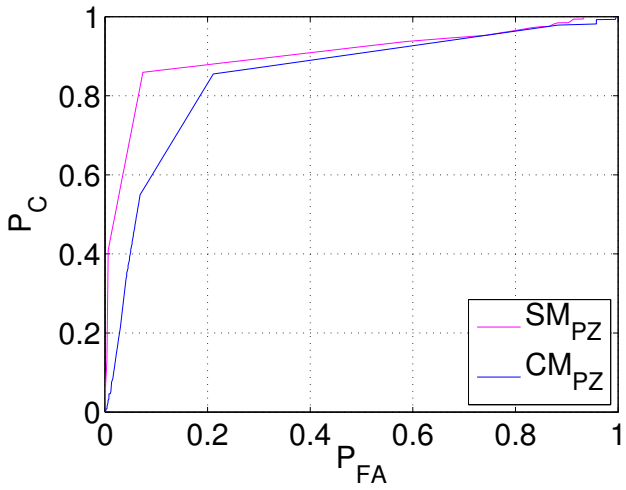

Figure 4.30: PZM order 6

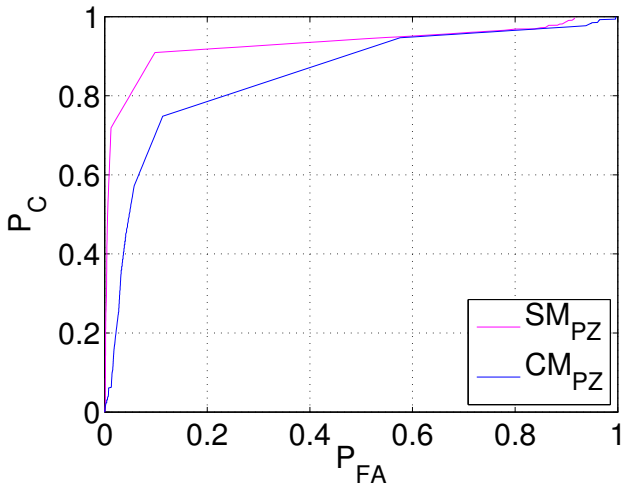

Figure 4.31: PZM order 8

In Fig. 4.30 it can be observed a slope steeper that it respond to the coefficients of order 6. With the same percentage than the previous graph, 20 % of false alarm, it is got a minimum of 80 % of probability of correct detection.

Fig. 4.31 achieves high values faster and it is improved the performance of spherical mines detection of previous graphic, while the data obtained on the cylindrical mines detection are slightly worse in the first middle of the graph of order 8.

Fig. 4.32 presents results better than the previous one, being very fast response to such spherical mines where we have a detection of 90 % with only 5 % of probability of false alarm. The values of the cylindrical mine detection also improve with regard to the previous chart.

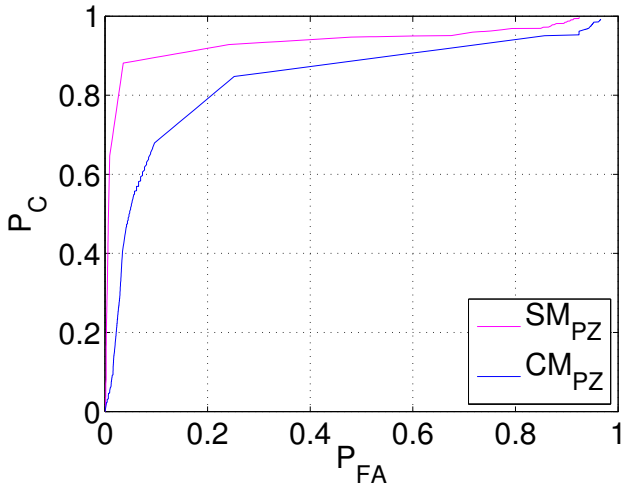

Figure 4.32: PZM order 10

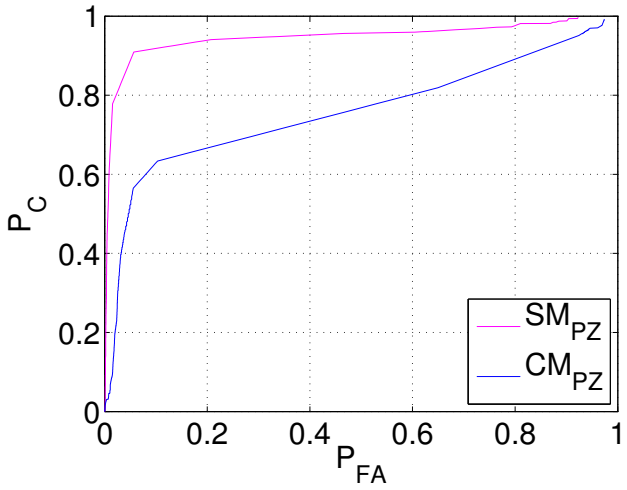

Figure 4.33: PZM order 12

And in the last figure of this group (Fig. 4.33), it can be seen as the values of spherical mine detection still get a little better, while the cylindrical mine detection is greatly affected, decreasing their results clearly.

As has been said it should be noted that these coefficients of order 12 are missing as follows: (11,1) and (12,0). As this chart is the last of this group, noting that the results can be determined that the coefficients of order 6, 8 and 10 are remarkably effective, being the order 6, since it has less coefficients, the most effective in terms of resources is concerned.

So as it has done previously, the next graphics that are displayed correspond to the selection of coefficients according to the diagram 4.9.

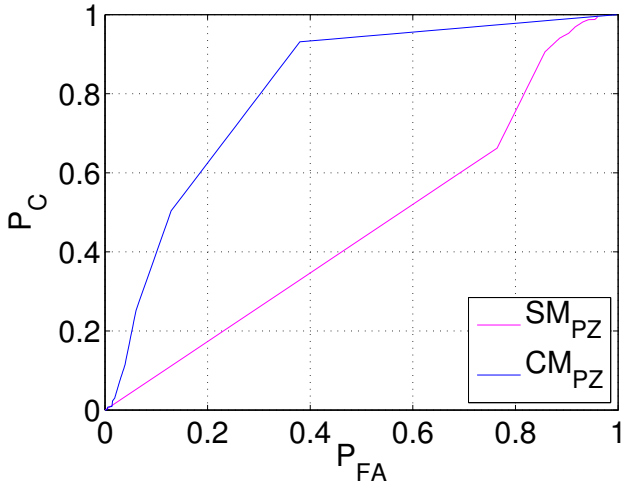

Figure 4.34: PZM n=0,1 m=0,1

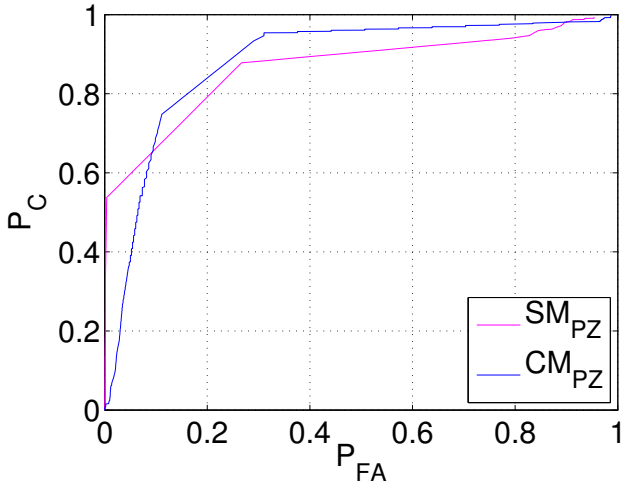

Figure 4.35: PZM n=0..2 m=0..2

In the first graph of this group (Fig. 4.34) it is had a bad detection in spherical mines while the cylindrical mine detection performs much better, thing that has not happened in previous figures.

Fig. 4.35 corresponds to coefficients (0,0), (1,0), (1,1), (2,0), (2,1) and (2,2). It gets very good results being the answer to the spherical mines very fast, in a few hundredths probability of false alarm, it is had 40 % of probability, and 90 % with only 15 % of probability of false alarm. The cylindrical mine detection is not less, and get a 80 % probability with a 20 % of false alarm rate. So they are very good results.

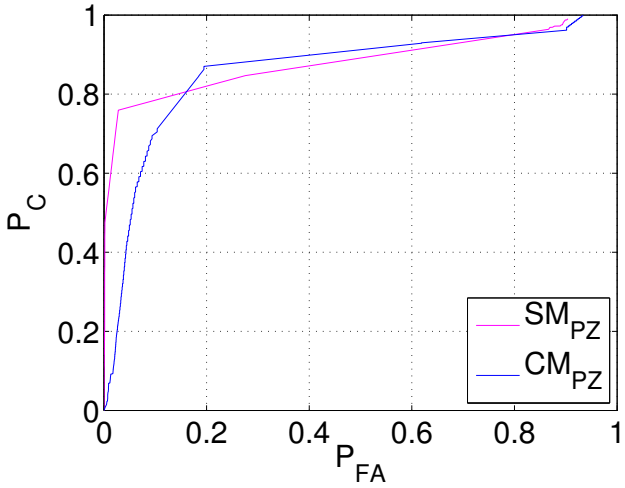

Figure 4.36: PZM n=0..3 m=0..3

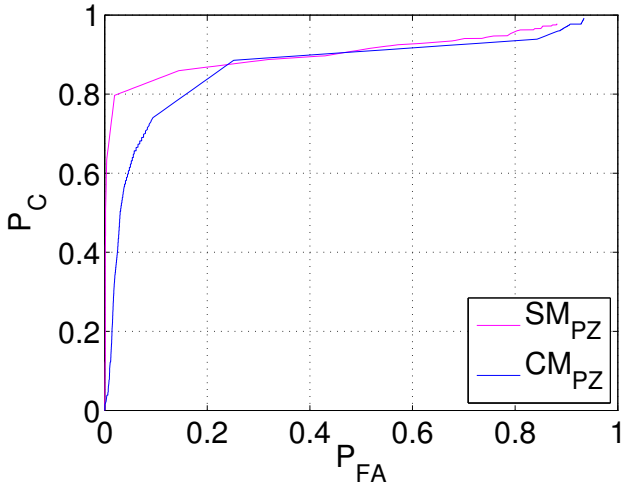

Figure 4.37: PZM n=0..4 m=0..4

If there are added the coefficients (3,1), (3,2) and (3,3) it is obtained as it can be seen in Fig. 4.36 an even faster response, and the early values where previously obtained 40 % confidence, we now have a 55 %, good data, however, that then is clouded to reach 80 % of probability when it is had 20 % of probability of false alarm. Results are very good, and it should be noted that the values of spherical and cylindrical mine detection resemble.

In the last figure of this section of PZM, are represented the results for the coefficients $n = 0..4$ and $m = 0..4$, the resulting values are very good, in part to overcome results of the previous chart, but the difference between the last two is not as great as in previous graphs. The speed of reaching a 80 % of confidence level increases considerably with a 10 % chance that the object is a mine. With these results are optimal implementation done.

Summarizing the discussed in this section, we note that the responses of the coefficients of order 6, 8 and 10 (4.30, 4.31 and 4.32) are very good, but if we want a quick response the last two graphs (4.36 and 4.37) are perfect. The overall results obtained in the implementation are very good and similar to Zernike ones too.

In this subsection it is discussed the results obtained for the Fourier Descriptors. As there is not relation with Zernike coefficients or Pseudo Zernike ones, they are explained individually or by groups of coefficients. In chapter 4.5 they are compared with the best results of the other two descriptors.

Fig. 4.38 shows images of the three types of underwater objects. Below, in Fig. 4.39 the FD of the previous images are drawn.

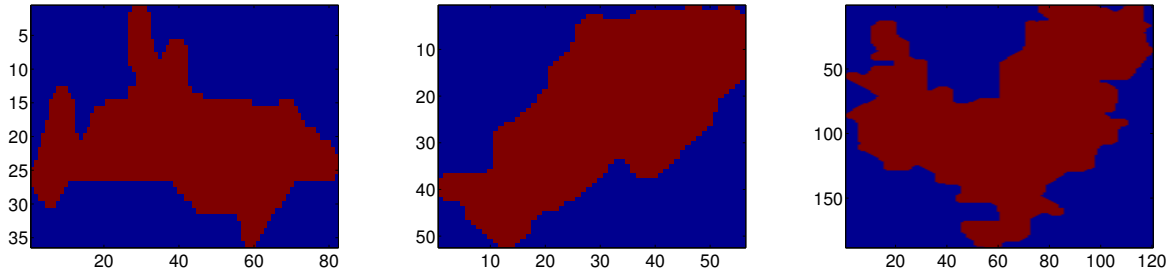

(a) Spherical mine (b) Cylindrical mine (c) No mine

Figure 4.38: Examples of different types of objects

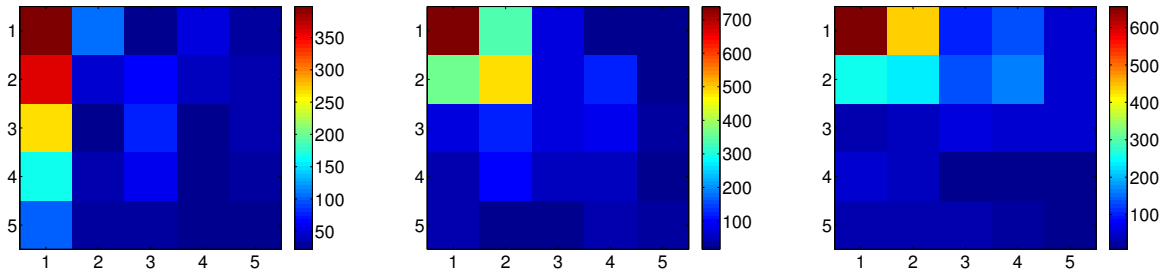

(a) FD for upper (b) FD for upper (c) FD for upper

Figure 4.39: FD obtained for 4.38

To begin, we should mention that we have worked with a database of 5x5 coefficients, sufficient for the work that concerns us, these range from 0 to 4 in each dimension. The graphs show the results for the independent coefficients (0,0), (0,1), (1,0), (0,2) and (2,0) which have the maximum information provided, and then as it has been done in the descriptors before, by groups that include square areas like the following diagram, each time adding the coefficients assigned by a new color.

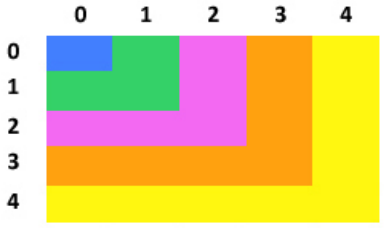

Figure 4.40: Coefficients chosen

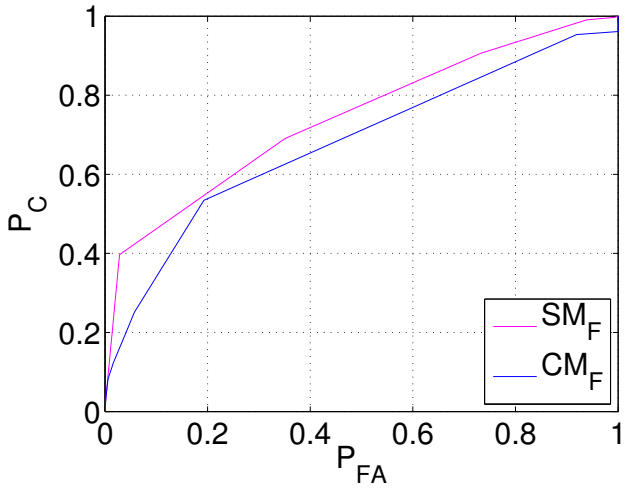

Figure 4.41: FD coefficient 0.0

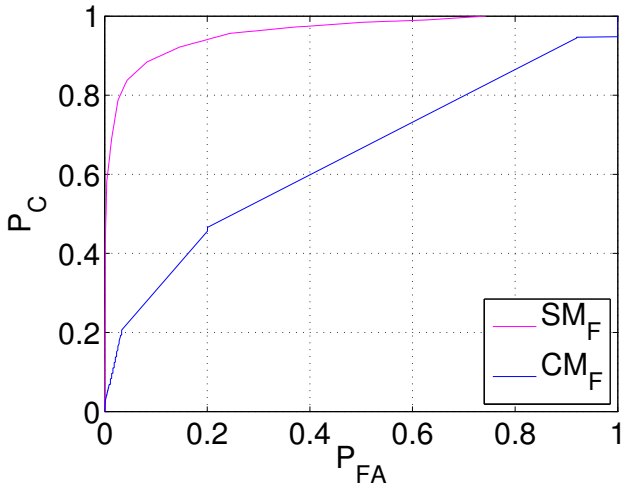

Figure 4.42: FD coefficient 0.1

The first coefficient (0,0) corresponds to Fig. 4.41. The probability of correct classification for the spherical mines (SM) is shown in magenta, and in blue for the cylindrical mines (CM). It gets results more acceptable than the Zernike and Pseudo Zernike in the corresponding coefficient, here we obtain results with a success of 50 % when we have a 20 % of probability of false alarm. It may also reflect the response of spherical mine is slightly above than the cylindrical one, which did not happen in the first coefficient of the other descriptors.

In the second figure of this section it is clearly seen as reacts the coefficient (0,1) in the detection of spherical mines as it goes to 90 % success rate with only 10 % of probability of false alarm. Until this moment this is the best result; but the result of cylindral mines is bad in comparison with the spherical mines mentioned.

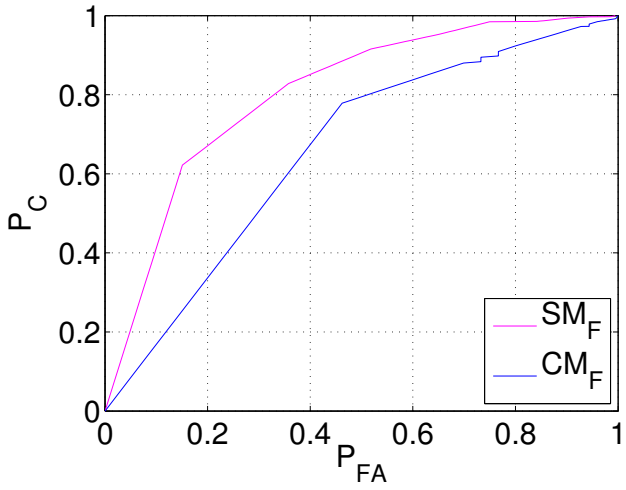

Figure 4.43: FD coefficient 0.2

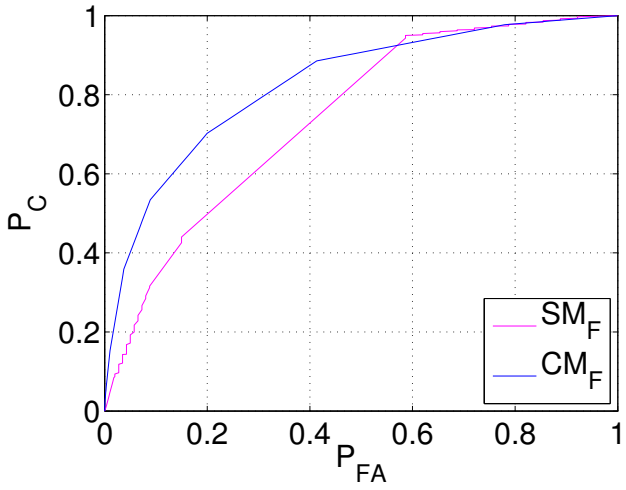

Figure 4.44: FD coefficient 1.0

In the Fig. 4.43 it is seen with easily that the results of spherical mine classifier outcomes worse, reaching a 90 % effective in the middle of the figure. However in the case of cylindrical mines, they improve reaching 80 % effectiveness in middle-figure and reaching the success of 100 % when we have 100 % of probability of false alarm, value we have not in the previous graphics.

Fig. 4.44 corresponds to the coefficient (1,0) and it gets a better response in cylindrical mines getting a 70 % of accuracy with 20 % of probability of false alarm. Although, the rate of spherical mine detection subsides and is slow for it to achieve high values of efficiency.

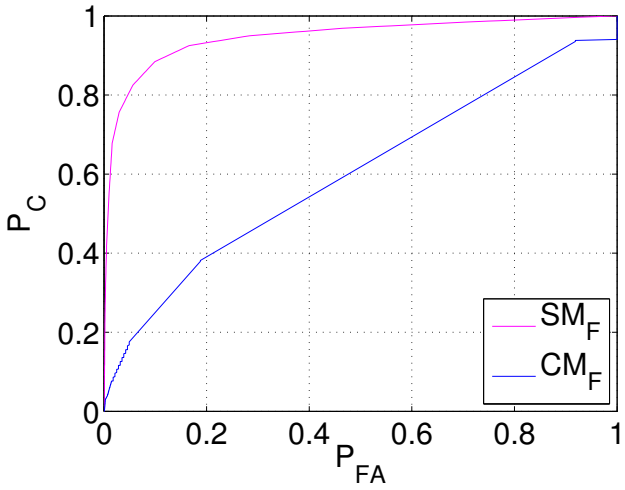

Figure 4.45: FD coefficient 2.0

The last coefficient analyzed individually is (2,0) and it corresponds to the figure at left (Fig. 4.45). It is seen that is very similar to Fig. 4.42 which corresponds to the coefficient (0,1). The values decrease in very small quantities on this figure regarding the one cited. And if the two types of mine are compared the difference between them is about 30 % in the chart's middle. But the important problem is that we still can not reach the total reliability when it is had 100 % of false alarm (only up to 95%).

Below are the figures for groups of coefficients selected according to the diagram 4.40. The first for the set of coefficients (0,0), (0,1), (1,0) and (1,1) (Fig. 4.46) and as it can be observed that it gets very good results, beating spherical and cylindrical mines detection a 90 % reliability with only 30 % of probability of false alarm.

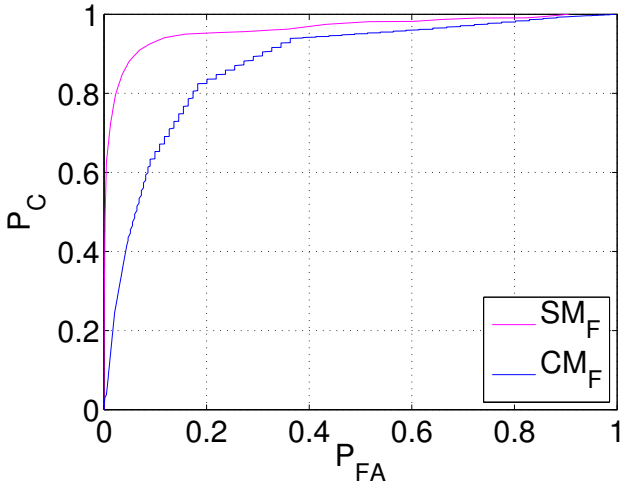

Figure 4.46: FD coeffs 0..1 x 0..1

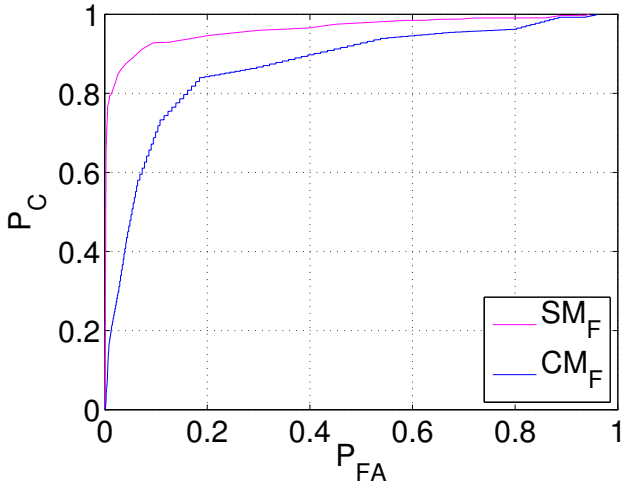

Figure 4.47: FD coeffs 0..2 x 0..2

The upper figure (Fig. 4.47) which is very similar to the one of its left (4.46) increases its coefficients with the addition of the following: (0,2), (1,2), (2,0), (2,1) and (2,2) to help get a quicker response up to 90 % of confidence to be a spherical mine with less than 10 % of probability

of false alarm. Regarding the cylindrical mines is also increased the speed of detection, while the values of the second part of the graph are a few hundreths lower.

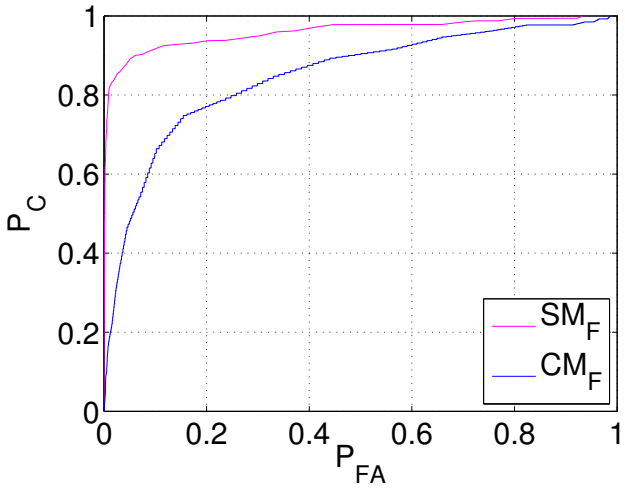

Figure 4.48: FD coeffs 0..3 x 0..3

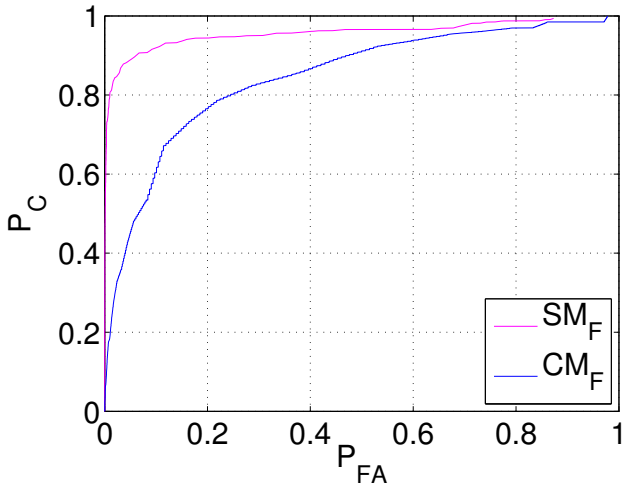

Figure 4.49: FD coeffs 0..4 x 0..4

The two figures above (Fig. 4.48 and Fig.4.49) correspond to the addition in the first, of the coefficients (0,3), (1,3), (2,3), (3,0), (3,1), (3,2) and (3,3), and the addition in the second of (0,4), (1,4), (2,4), (3,4), (4,0), (4,1), (4,2), (4,3) and (4,4). The similarity between the two figures is evident, as the diferences of those values are minimal, so that improvements in results are negligible. Continue making a very rapid response to spherical mine and cylindrical mine.

In this section coefficients have been analyzed separately and then by groups. It has obtained some clear results that to obtain a good classification of the mine in question, has to use more than one value, because only one coefficient is good for only one type of mine, not both. However if it is taken a set of coefficients such as the first graph of this type (Fig. 4.46) consisting of the first four coefficients, is shown that the results are very accurate for the classification of the two types of mines. It should also be noted that introducing more coefficients does not mean the improvement of effectiveness, since it reaches a point that it is unnecessary to add more.

4.5 Comparative of best results

In this section it is discussed about the conclusion and the best results from the descriptors: ZM, PZM and FD.

The following graphs are considered that provide the best improved reliability of implementations in each of its categories.

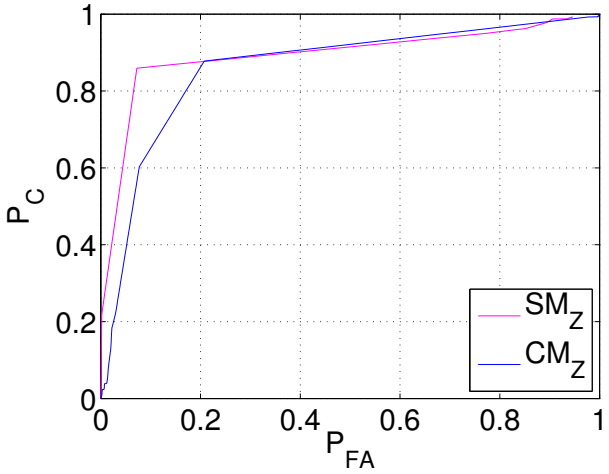

Figure 4.50: Best ZM (coefficients n=0..2 m=0..2)

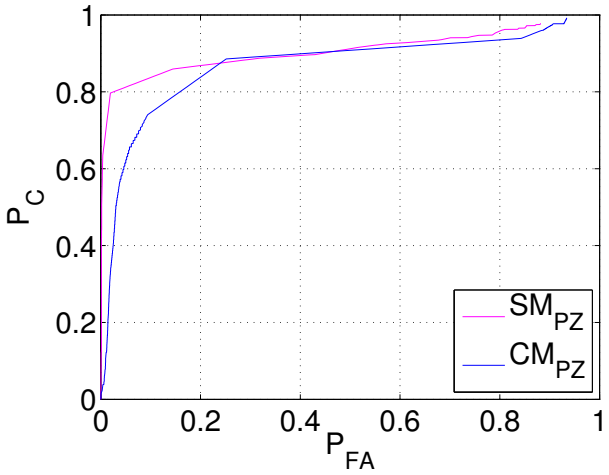

Figure 4.51: Best PZM (coefficients n=0..4 m=0..4)

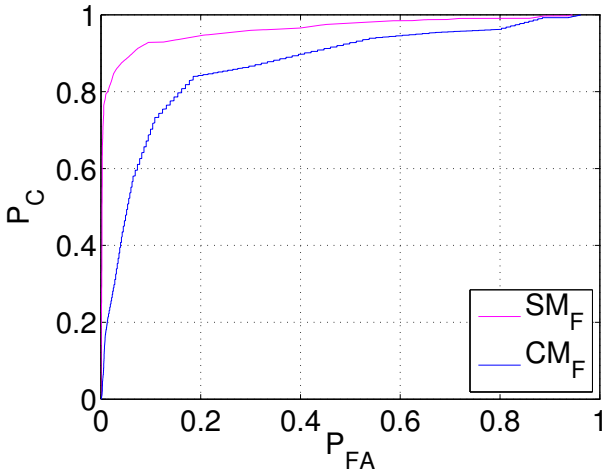

Figure 4.52: Best FD (coefficients 0..2 x 0..2)

The first figure (Fig. 4.50) corresponds to the ZM for coefficients: (0,0), (1,1), (2,0) and (2,2). The middle figure (Fig. 4.51) represents the PZM for coefficients (0,0), (1,0), (1,1), (2,0), (2,1), (2,2), (3,0), (3,1), (3,2), (3,3), (4,0), (4,1), (4,2), (4,3) and (4,4). And the last figure (Fig. 4.52) on the previous page shows the results of the FD for coefficients (0,0), (0,1), (0,2), (1,0), (1,1), (1,2), (2,0), (2,1) and (2,2).

It can be seen that the three are working properly reaching values close to 80 % of confidence in both types of mines with only 20 % of probability of false alarm.

Is also seen as the answers are faster with PZM and FD than ZM, which takes longer to reach high levels.

Note that these three graphs correspond to coefficientes chosen by the diagrams (Fig. 4.8, Fig. 4.9 and Fig. 4.40) rather than established by order of the coefficients.

Given these results would be hard to pick a favorite, but if one takes into account the implementation easier and faster the best response is FD.

The tables below show the confusion matrix belonging to different thresholds for the previous figures.

The tables below show the confusion matrix belonging to different thresholds for the previous graphics.

In these confusion matrix it has been chosen taking approximately 10 % of false alarm probability. The red colour represents the objects that being a mine are considered as no mine, these are called missclassifications. In orange colour are represented the cases when a no mine is considered as a mine, it means, a false alarm.

	C	S	N
C	67	29	35
S	46	249	25
N	292	250	3326

Table 4.1: Zernikes 3x3 (threshold used 51, 50)

	C	S	N
C	92	1	38
S	67	200	53
N	333	37	3498

Table 4.2: PZernikes 5x5 (threshold used 53, 49)

	C	S	N
C	73	24	34
S	29	267	24
N	339	95	3434

Table 4.3: Fourier 3x3 (threshold used 51, 51)

The table owned by ZM shows how it behaves better for the spherical mines than for spherical mines. In the next table corresponding to the PZM it can be seen that for cylindrical mines the outcome is better than for the spherical ones. And finally, in the confusion matrix of FD, the results are better for the spherical mines than the cylindricals.

The results of the confusion matrix displayed look different from the previous figures, this is due to the interpolation performed in the graphics and the large quantity of data obtained from the multiple thresholds used.

5 Conclusion

In this thesis, the workflow of description and classification of objects for underwater sonar images is presented. The calculation of descriptors requires low times of processing.

Three different kinds of descriptors have been considered: Zernike moments, pseudo Zernike moments and Fourier Descriptors. Then the Mahalanobis classifier is applied, assuming that the feature vectors have gaussian distribution and based on the leave-one-out method.

The global descriptors and classifiers are expected to benefit strongly from a more advanced segmentation algorithm as this might result in a better classification.

The aim of this work is to obtain the best response in the automatic classification of underwater objects. For this reason, the important thing is that the implementation works well in the classification of mines with a low probability of false alarm.

One example of good results is that, with FD it is obtained with only 10 % of probability of false alarm a success rate of 92 % and 70 % of spherical mines and cylindrical mines detection respectively.

This thesis has interest because in real life the location of underwater objects is very important. Because a wrong detection of a mine entails a high cost in human lives and economic terms as it has been said, so we need to look for the best results we can get.

Therefore the results are very good and fast, but improvement is still necessary; either in the pre-segmentation of objects, or whether the phases carried out in this work, using better descriptors or some other classifiers, or maybe, not assuming Gaussianity for the features.

Bibliography

[1] Castellano A. and Gray B. Autonomous interpretation of side scan sonar returns. Proceedings of the Sympsosium on Autonomous Underwater Vehicle Technology, pages 248 – 253, 1990.

[2] Trucco A. and Murino V. Edge/region-based segmentation and reconstruction of underwater acoustic images by markov random fields, 1998.

[3] Bhatia A. B. and Wolf. E. Proc. comb. phil. soc. J. Optical Soc. Am., 50:40 – 48, 1954.

[4] S. Banks. Signal Processing, Image Processing and Pattern Recognition. Prentice-Hall, Englewood Cliffs, NJ, 1990.

[5] D. Boulinguez and A. Quinquis. Classification of underwater objects using Fourier descriptors. In Proceedings of the International Conference on Image Processing and its Applications, pages 240 – 244, 1999.

[6] Delvigne J. C. Shadow classification of underwater using neural networks. 4th Undersea Defence Conference, pages 214 – 221, 1992.

[7] Zahn C.T. and Roskies R.Z. Fourier descriptors for plane closed curves. IEEE Trans. Computers, C - 21(3):269 – 281, 1971.

[8] Gerald J. Dobeck, John C. Hyland, and Le'Derick Smedley. Automated detection and classification of sea mines in sonar imagery. In Society of Photo-Optical Instrumentation Engineers (SPIE) Conference Series, volume 3079, pages 90–110, 1997.

[9] M.F. Doherty, J.G. Landowski, P.F. Maynard, G.T. Uber, D.W. Fries, and F.H. Maltz. Side scan sonar object classification algorithms. In Proceedings of the 6th International Symposium on Unmanned Untethered Submersible Technology, pages 417 –424, 1989.

[10] Persoon E. and Fu K.S. Shape discrimination using fourier descriptors. IEEE Trans. Systems, Man and Cybernetics, SMC - 7(3):170 – 179, 1977.

[11] Zernike F. Physica. 1:689, 1934.

[12] J. A. Fawcett. Image-based classification of sidescan sonar detections. In Proceedings of the CAC/CAD Conference, 2001.

[13] R. C. Gonzalez and R. E. Woods. Digital Image Processing. Addison-Wesley Longman Publishing Co., Inc., Boston, MA, USA, 2001.

[14] J. Groen, E. Coiras, and D. Williams. Detection rate statistics in Synthetic Aparture Sonar images. In Proceedings of the Underwater Acoustic Measurements Conference, 2009.

[15] Ming-Kuei Hu. Visual pattern recognition by moment invariants. IRE Transactions on Information Theory, 8(2):179 – 187, 1962.

[16] Besag J. On the statistical analysis of dirty images. Journal of the Royal Statistical Society, B-48:259 – 302, 1986.

[17] S. G. Johnson and A. Deaett. The application of automated recognition techniques to side-scan sonar imagery. Journal of Oceanic Engineering, 19:138 – 144, 1994.

[18] F. Langner, C. Knauer, W. Jans, and A. Ebert. Side scan sonar image resolution and automatic object detection, classification and identification. In Proceedings of the OCEANS Conference, pages 1 – 8, 2009.

[19] Luciano and Roberto M. Cesar. Shape Analysis and Classification: Theory and Practice (Image Processing Series). CRC Press, Taylor & Francis Group, 6000 Broken Sound Parkway NW, Suite 300, 2000.

[20] Luciano and Cesar R. M. Shape Analysis and Clasification: Theory and Practice (Image Processing Series). 6000 Broken Sound Parkway NW, Suite 300, 2000.

[21] Frederic Maussang, Michèle Rombaut, Jocelyn Chanussot, and Maud Amate. Fusion of local statistical parameters for buried underwater mine detection in sonar imaging. EURASIP Journal on Advances in Signal Processing, 2008, 2008.

[22] H. Midelfart, J. Groen, and O Midtgaard. Template matching methods for object classification in synthetic aperture sonar images. In Proceedings of the Underwater Acoustic Measurements Conference, 2009.

[23] M. Mignotte, C. Collet, P. Pérez, and P. Bouthemy. Hybrid genetic optimization and statistical model based approach for the classification of shadow shapes in sonar imagery. IEEE Transactions on Pattern Analysis and Machine Intelligence, 22:129 – 141, 2000.

[24] Kuhl F. P. and Giardina C. R. Eliptic Fourier features of chosed contours. echnical Report, Arradcom, Dover, NJ, 1981.

[25] M. Peura and J. Iivarinen. Efficiency of simple shape descriptors. In In Aspects of Visual Form, pages 443 – 451. World Scientific, 1997.

[26] W. Pieczynski. Statistical image segmentation. Machine Graphics and Vision, 1:261 – 268, 1992.

[27] I. Quidu, J. Ph. Malkasse, G. Burel, and P. Vilbé. Mine classification based on raw sonar data: an approach combining Fourier descriptors, statistical models, and genetic algorithms. In Proceedings of IEEE Oceans Conference, volume 1, pages 285 – 290, 2000.

[28] I. Quidu, J.P. Malkasse, G. Burel, and P. Vilbe. Mine classification using a hybrid set of descriptors. In Proceedings of the OCEANS Conference, volume 1, pages 291 – 297, 2000.

[29] Burel G. Quidu I., Malkasse J. and Vilve P. Mine classification using a hybrid set of descriptors. Proceedings of the Oceans Conference, 1:291 – 297, 2000.

[30] Balasubramanian R. and Stevenson M. Pattern recognition for underwater mine detection. 2001.

[31] Castleman K. R. Digital image processing. Practice-Hall, Englewood Cliffs, New Yersey, 1996.

[32] Chelappa R. and Bagdazian R. Fourier coding of image boundaries. IEEE Trans. Pattern Analysis and Machine Intelligences, PAMI - 6(1):102 – 105, 1984.

[33] Teague M. R. Image analysis via the general theory of moments. J. Optical Soc. Am., 70:920 – 930, Aug. 1980.

[34] S. Reed, Y. Petillot, and J. Bell. An automatic approach to the detection and extraction of mine features in sidescan sonar. IEEE Journal of Oceanic Engineering, 28:90 – 105, 2003.

[35] S. Reed, Y. Petillot, and J. Bell. Automated approach to classification of mine-like objects in sidescan sonar using highlight and shadow information. IEE Proceedings - Radar, Sonar and Navigation, 151:48 – 56, 2004.

[36] Lane D. Tena Ruiz I. and Chantler M. A comparison of inter-frame feature measures for robust object classification in sector scan sonar image sequences. IEEE Journal of Oceanic Engineering, 24:458 – 469, 1999.

[37] Anderson T. W. An introduction to multivariate statistical analysis. John Wiley and Sons, Inc., 1984.

[38] D. Zhang and G. Lu. Review of shape representation and description techniques. Pattern Recognition, 37(1):1 – 19, 2004.